Journal of Energy Storage 84 (2024) 110977

Contents lists available at ScienceDirect

Journal of Energy Storage

journal homepage: www.elsevier.com/locate/est

Research papers

Investigating the effectiveness of borophene on anchoring and influence on kinetics of sodium superoxide in sodium–oxygen batteries

C. Fwalo [a,b,*], A. Kochaev [c], R.E. Mapasha [a]

[a] Department of Physics, University of Pretoria, Pretoria, South Africa
[b] Department of Physics, Copperbelt University, Kitwe, Zambia
[c] Research and Education Center "Silicon and Carbon Nanotechnologies", Ulyanovsk State University, Ulyanovsk, Russia

ARTICLE INFO

Keywords:
Density functional theory
Sodium–oxygen battery
χ_3-borophene
β_{12} borophene
Sodium superoxide

ABSTRACT

Owing to the increasing cost and limited resources of lithium metal, there is a growing interest in developing energy storage systems that are more affordable, environmentally friendly, and have high energy densities. This is also driven by the need to significantly reduce carbon dioxide emissions resulting from the use of fossil fuels. The sodium–oxygen battery has emerged as a potential alternative, as the materials used for both of its electrodes are among the most abundant and inexpensive elements on Earth. However, despite these advantages, there are technical challenges in implementing it, such as the insulation of the cathode electrode and failure to prevent discharge products from desorbing into electrolytes during discharging. In this study, using density functional theory based on first principles, we investigated the electronic properties of free-standing β_{12} and χ_3-borophenes after adsorption of sodium superoxide (NaO_2). Our findings showed that the adsorption energy of sodium superoxide on β_{12} and χ_3 borophene are −3.85 eV and −3.24 eV, respectively. The large negative values of adsorption energy suggest that sodium superoxide is anchored spontaneously, which is significant as it can be prevented from migrating to the negative electrode via the electrolyte during the discharging process. Furthermore, the β_{12} and χ_3 structures showed moderate diffusion energy barriers of 0.89 eV and 1.37 eV and decomposition energies of 0.73 eV and 0.52 eV, respectively. The latter demonstrates the catalytic effects of nanosheets on the decomposition of the sodium superoxide into separated sodium (Na^+) and oxygen (O_2). Moreover, the decomposition energies being lower than sodium superoxide formation energy (3.90 eV) in a vacuum, suggests nanosheets effects during the charging process. Most importantly, the metallic characteristics of both crystal structures were preserved after the adsorption of sodium superoxide, and the electronic conductivities were enhanced. This is significant to improve the cycle life of the battery, as the materials can charge back the decomposed species during the charging process, thereby preventing the formation of dendrites at the surface of the cathode. Ultimately, the predicted electronic properties for both structures demonstrate their potential as cathode electrode materials for enhancing the electrochemical processes of sodium–oxygen batteries.

1. Introduction

For the drastic effect of climate change due to high levels of carbon dioxide emission to be significantly reduced, communities need energy-storing systems that could exceed the current technology of lithium batteries. To date, the lithium-ion battery is the most used energy-storing device due to its lightweight, high energy, and high power density [1]. It has been used in most portable devices [2] and as energy storage in electric vehicles (EVs) [3] to mention but a few. However, due to the rapid advancements in technology, it cannot meet the growing demand. Owing to that, researchers have started considering energy-storing systems that could surpass lithium-ion battery technology [4]. Because of the ultra-high theoretical capacities and energy densities of the alkali metal–oxygen batteries, they have been identified as an alternative to lithium-ion battery inability. Among all the metal–oxygen batteries, the lithium–oxygen battery by far has the highest theoretical capacity and reduced operational costs. This is because one of the active materials (oxygen) for the porous cathode electrode, comes from the ambient environment [5–7].

Despite having ultra-high theoretical capacity, lithium–oxygen battery faces challenges restricting it from being practically implemented, and among the challenges is high over-potential during the charging process. This implies that more energy is needed during the charging

* Corresponding author at: Department of Physics, University of Pretoria, Pretoria, South Africa.
E-mail address: fwalochewe99@gmail.com (C. Fwalo).

https://doi.org/10.1016/j.est.2024.110977
Received 16 December 2023; Received in revised form 27 January 2024; Accepted 15 February 2024
Available online 20 February 2024

process than the one realized during the discharging process. Consequently, many system components are worn out, leading to low energy efficiency and poor cycling life [5,8]. With the mentioned challenges, the sodium–oxygen battery has been identified as a potential alternative to the lithium–oxygen battery due to the similarity of their electrochemical processes [9]. One of the advantages of the sodium–oxygen battery is that it has low over-potential during charging, which is due to the reversible electro-chemistry of sodium superoxide (NaO_2) formed during the discharging process [9,10]. This feature allows the battery to have high energy efficiency because not much energy is required to decompose NaO_2 during the charging process. Therefore enhancing the cycling life of the battery. Furthermore, sodium, which is used as the negative electrode, is one of the most abundant elements on Earth, making the system more affordable [11]. The cathode electrode consists of oxygen, which is also among the most abundant and affordable elements on Earth. Typically, during the discharging process, oxidation occurs at the anode while sodium ions move to the cathode and oxygen molecules move into the battery. At the cathode, sodium and oxygen combine to form sodium superoxide as a single molecule. Conversely, during the charging process, this process occurs in reverse [10].

Regardless of the advantages of sodium–oxygen batteries, there are technical issues including poor electronic transport, clogging of discharge products at the surface of the cathode electrode, and poor kinetics of insoluble and non-conductive discharge products [12]. Additionally, the high chemical reactivity of sodium metal (anode) makes it react with desorbed NaO_2. Scientists and engineers are working on finding materials that could be used as cathode electrodes and mitigate these challenges. One critical question is how to retain most of the discharge products of sodium superoxide and prevent them from diffusing to the negative electrode via the electrolyte during the discharging process [10]. With these observations in mind, researchers are working on realizing a practical system future.

Sodium–oxygen batteries commonly use porous carbon as a cathode electrode, but the discharge products tend to clog the pores and block reaction sites, leading to battery failure [13]. Researchers have turned to 2D materials to address these issues due to their high surface area, and other unique properties such as good metallic characteristics and mechanical and physical capabilities [14,15]. Some 2D materials being investigated and used as electrode materials include graphene [16,17], hexagonal Boron Nitride (2D-hBN) [18,19], and Mxenes [20,21].

Researchers led by Mannix successfully synthesized crystalline monolayer boron sheets on silver surfaces using ultrahigh vacuum conditions [22]. Since then, borophene has received significant attention, leading to the fabrication and synthesis of many polymorphs of its kind [23]. Feng and his team used first principles and experimental approaches to synthesize and confirm 2D boron polymorphs of β_{12} and χ_3-borophenes on an Ag(111) substrate [24]. These experimentally realized borophenes possess unique properties such as excellent mechanical stability [25] and good electronic transport [26,27]. Additionally, the calculations of phonon dispersions and analysis of frequency modes have indicated that the borophenes are kinetically stable at the ground state (0 K), as the frequency modes are zero. This suggests that borophenes are dynamically stable [25]. Furthermore, the use of ab initio molecular dynamics (AIMD) has shown that the structures have minimal distortions even at extreme temperatures of up to 1000 K [28], suggesting that they are thermodynamically stable.

These exceptional properties make them suitable for various electronic applications, including anodes in lithium-ion batteries [29], sensing toxic gases [30–32], and water splitting in fuel cells [33]. With the noted successes and exceptional performance of borophene materials as anode electrode materials in lithium-ion batteries, there have been theoretical predictions that they could also be utilized as cathode electrodes in sodium and lithium-sulfur batteries [34–37]. While there are numerous reported applications of β_{12} and χ_3-borophenes as potential electrode materials in batteries, there is scarce information about their use as cathode electrode materials in sodium–oxygen batteries and how they affect sodium superoxides which are the main discharge products.

In the present work, using the density functional theory (DFT) approach, we explored the adsorption mechanisms of sodium superoxide on β_{12} and χ_3-borophenes as cathode electrode materials for improved performance of sodium–oxygen batteries. Firstly, we computationally optimized the two experimentally synthesized 2D boron polymorphs (β_{12} and χ_3-borophene) and generated NaO_2 configurations, then fully optimized them to determine the most energetically stable configurations. Next, we systematically calculated diffusion energy barriers and decomposition energies of NaO_2 on both structures to determine rates of discharging and charging processes. Lastly, we investigated NaO_2-borophene electronic interactions by calculating the charge density differences and quantified charge density. Additionally, we calculated the density of states (DOS) and bands structures to understand the effects of adsorbates on the electronic structures of the crystals.

2. Computational methods

In this study, we used the quantum ESPRESSO code [38] to conduct all the density function theory (DFT) simulations. We employed the spin-polarized generalized gradient approximation (GGA) [39] within the functional of Perdew–Burke–Ernzerhoff (PBE) [40] to treat the exchange and correlation energy of the electron's interactions in the crystals. We used the projector augmented wave (PAW) potential [41] as the type of pseudo-potential to describe the core electrons. After conducting convergence tests, we set a kinetic energy cut-off of 50 Ry and used a plane-wave basis set to obtain the ground state energies for both crystal structures. In addition, we used the Monkhorst–Pack scheme [42] with a K-points sampling of $13 \times 9 \times 1$ for β_{12}-borophene and $16 \times 11 \times 1$ for χ_3-borophene within the Brillouin zone [43]. We conducted geometrical relaxation of the structures until all atomic positions had converged within an energy difference of 10^{-5} eV and a Hellman–Feynman force convergence set to 10^{-6} eV/Å. We adopted the Methfessel and Paxton (MP) occupational function [44] to smear off the electrons and introduced spin-orbital polarization in every self-consistency field (SCF) calculation to treat magnetic effects if any. To account for the effects of van der Waals forces, we used DFT-D3 correction with the Grimme scheme [45]. Since adsorbates were crucial in all our simulations and to avoid the effects of repulsion forces, we generated and modeled supercells of sizes $3 \times 2 \times 1$ (30 boron atoms) and $4 \times 1 \times 1$ (32 boron atoms) for both crystal structures (β_{12} and χ_3-borophenes). To avoid periodic images from interacting, we used a vacuum space of 15 Å along the z-axis in all our calculations.

3. Results and discussions

3.1. Relaxed crystal structures for β_{12} and χ_3-borophenes

When making predictions about electronic properties, the structural properties of crystal structures are very critical. Therefore, we modeled and generated crystal structures of β_{12} and χ_3-borophenes, based on the space group of Pmmm2 and Cmmm, respectively. We used an orthorhombic crystal system for both structures. After a full optimization, we found that both structures were flat and had no corrugations. For β_{12}-borophene, the optimized lattice parameters were **a** = 2.920 Å and **b** = 5.095 Å with 5 atoms per unit cell and a hollow. For χ_3-borophene, the optimized lattice parameters were **a** = 2.909 Å and **b** = 8.393 Å with 8 boron atoms per unit cell and 2 hollows. In terms of symmetry orientation, both structures consist of parallel chains of hollow hexagons separated by chains of triangles of boron atoms (Fig. 1). The calculated lattice parameters agreed well with previously reported first principles results [46–49].

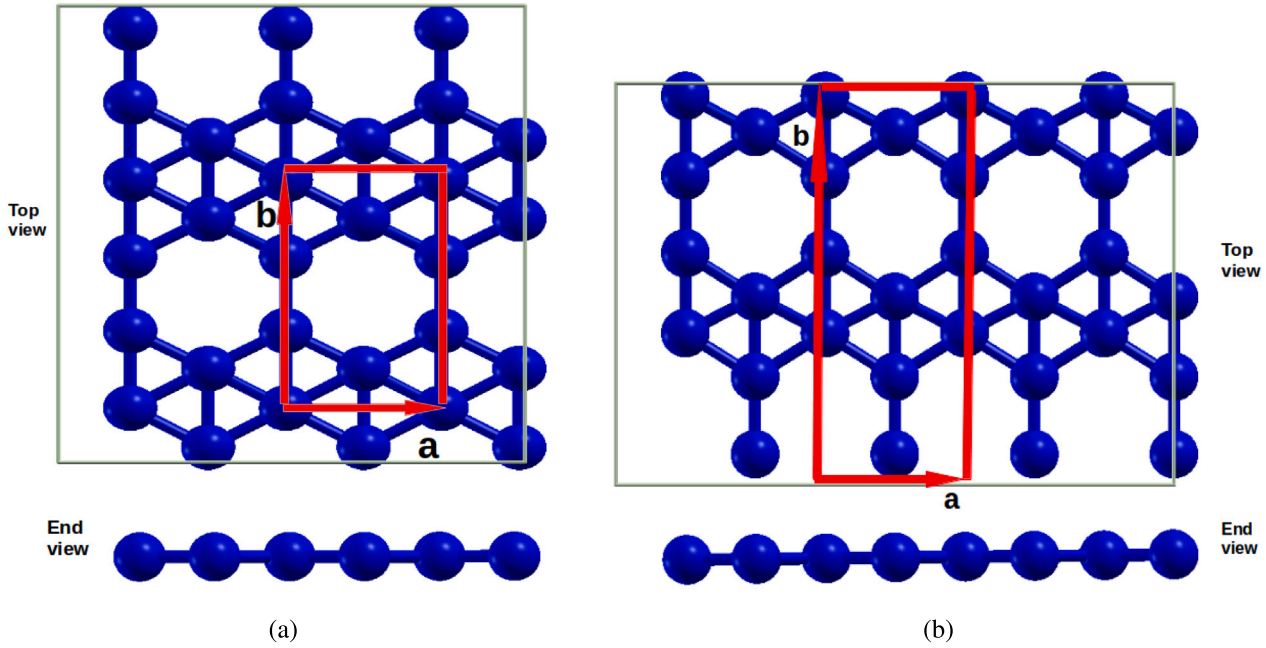

Fig. 1. Relaxed crystal structures top and end views: (a) β_{12}-borophene with a unit cell consisting of 5 boron atoms and single hollow (b) χ_3-borophene with a unit cell consisting of 8 atoms with two hollows. All the boron atoms are presented with the color blue and unit cells enclosed in red rectangles. (For interpretation of the references to color in this figure legend, the reader is referred to the web version of this article.)

3.2. Adsorption and charge densities of sodium superoxide (NaO_2) on β_{12} and χ_3-borophenes

After generating the nanosheets of β_{12} and χ_3 borophenes, we identified and added NaO_2 at different possible adsorption sites (Figs. 2a and 3a). Then we relaxed the systems to get the most stable configurations. Thereafter, we calculated the adsorption energies and compared the values to determine the most energetically stable configurations. The following equation was used:

$$E_{ads} = \frac{E_{complex} - E_{pure} - n(E_{adsorbate})}{n}. \quad (1)$$

Where E_{ads} is the adsorption energy of the material, $E_{complex}$ is the total energy of the nanosheet with the adsorbate, E_{pure} is the total energy of the nanosheet without an adsorbate, $E_{adsorbate}$ is the total energy of the adsorbate of interest, and n is the number of adsorbates anchored by the nanosheet.

3.2.1. Sodium superoxide (NaO_2) on β_{12}-borophene

Firstly, for the NaO_2 on β_{12}-borophene, we investigated four possible adsorption sites, as shown in Fig. 2: (b) Site 1, with the sodium atom situated on top of the hollow and oxygen atoms on top of the bridge, (c) Site 2, with the sodium atom on top of the bridge and oxygen atoms on top of the hollow, (d) Site 3, with the sodium atom on top of the boron atom and oxygen atoms on top of the hollow, and (e) Site 4, with the sodium atom on top of the boron atom at the center of the hexagon and oxygen atoms on top of the boron atom bonded to the bridge between the hollow hexagons.

After fully relaxing the systems, apart from the configuration at Site 4 (Fig. 2e) which drifted slightly on top of the oxygen atoms, other configurations remained in their positions and orientations. In particular, the configuration at Site 1 (Fig. 2b) and Site 4 (Fig. 2e) were pulled very close toward the surface of the β_{12} borophene, until oxygen atoms formed covalent bonds with boron atoms. After calculating the adsorption energies and binding distances (Table 1), we found that among the configurations closest to the nanosheet. The configuration at Site 1 (O_2 = 1.53 Å and Na = 2.54 Å) had the largest negative adsorption energy (−3.85 eV). These results suggest that this configuration (Fig. 2b) is the most energetically stable and strongly interacts with the monolayer.

3.2.2. Sodium superoxide (NaO_2) on χ_3-borophene system

Furthermore, we focused on the sodium superoxide on χ_3-borophene, as shown in Fig. 3. Here, we considered three possible sites: Site 1, the sodium atom is on top of the hollow and the oxygen molecule is on top of the bridge with the axis parallel to the boron atoms; Site 2, the oxygen molecule is on top of the hollow, and the sodium atom is on top of the bridge; and Site 3, the oxygen molecule is on top of the hollow and the sodium atom is on top of the boron atom.

After fully relaxing the systems, we found the configurations to have maintained their positions, except for the one at Site 3 which changed the orientation and diffused towards the bridge (Fig. 3c), demonstrating that its position was unfavorable. Additionally, the configuration with the sodium atom on top of the hollow was pulled strongly closer to the substrate, and oxygen atoms formed covalent bonds with boron atoms (Fig. 3a). Furthermore, the configuration at Site 2 also formed the covalent bond with the boron atoms (Fig. 3b) and very interestingly the adsorption energy was found to be almost equivalent to that of Site 1. This was obtained after we calculated the adsorption energies and binding distances to gain insight into the interactions (Table 1). The adsorption energies ranged from −3.70 to −2.04 eV. The binding distances ranged from 1.50 to 1.92 Å for O_2 and Na, and 2.23 to 2.65 Å between the nanosheet and NaO_2. Based on these results, the configuration at Site 1 was found to have spontaneous adsorption energy (−3.70 eV) and the shortest binding distance (O_2 = 1.50 Å and Na = 2.53 Å), supporting the formation of covalent bonds and indicating that the configuration at Site 1 is most energetically stable among others.

3.3. Diffusion and decomposition of sodium superoxide (NaO_2) on β_{12} and χ_3 borophenes

Typically, in batteries species migrate from the anode to the cathode and vice versa. During the discharging process, the sodium superoxide is formed at the surface of the cathode electrode and diffuses across toward the most stable adsorption site. Therefore, to ensure optimal performance, it is very significant to investigate the diffusion energy barrier of the material used as a cathode electrode. Additionally, understanding the decomposition of the discharge products at the surface of

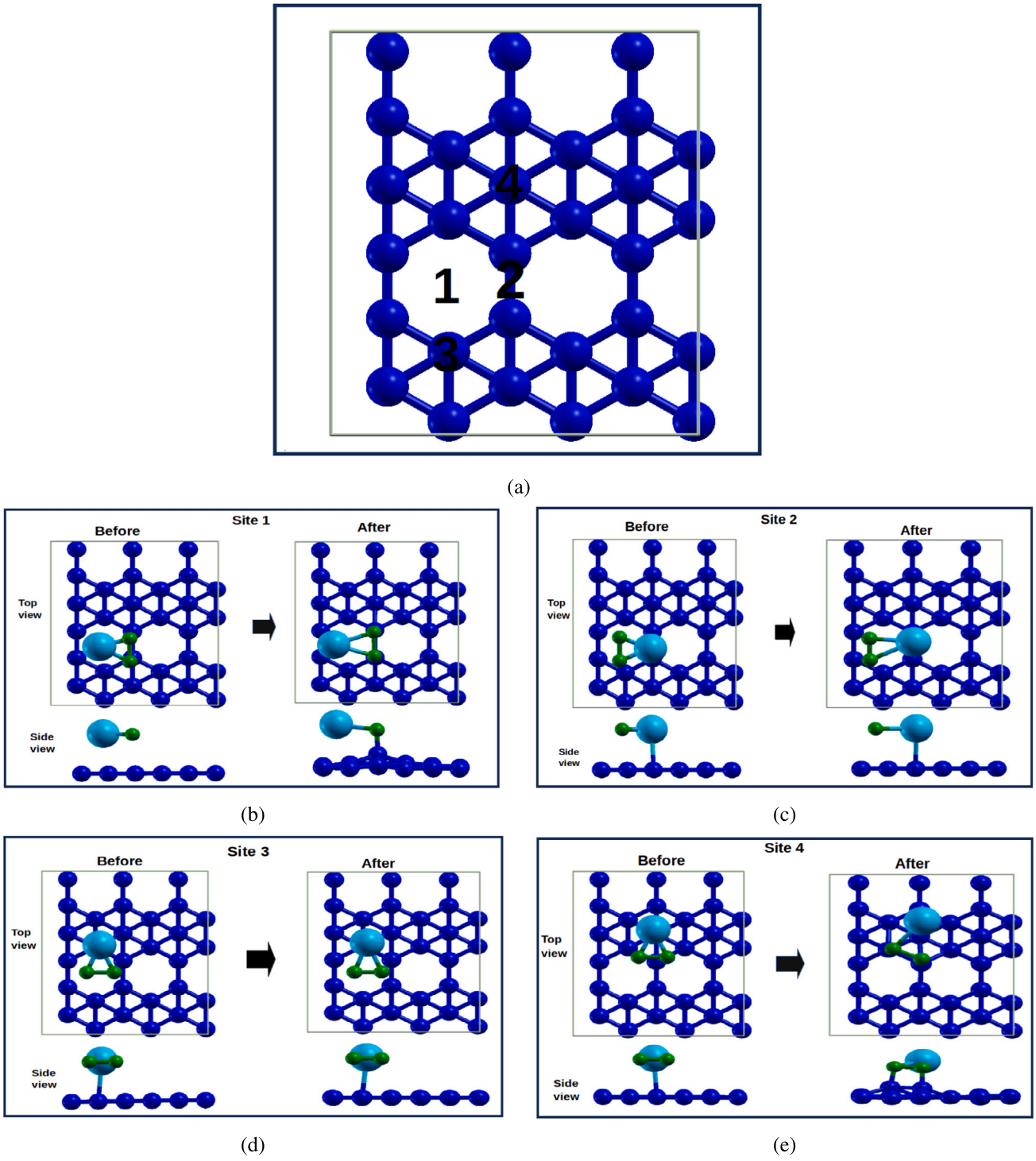

Fig. 2. Before (left) and after (right) simulations of NaO_2 on β_{12}-borophene systems: (a) Possible adsorption sites on β_{12} borophene (b) Top and end views of configuration at SITE 1, (c) Top and end views of configuration at Site 2 and (d) Top and end views of configuration at Site 3. The sodium, oxygen, and boron atoms are denoted by teal, green, and blue colors. (For interpretation of the references to color in this figure legend, the reader is referred to the web version of this article.)

the cathode electrode is very important. Therefore, using nudged elastic band (NEB) approach [50,51], we calculated the diffusion energy barrier and decomposition energy for β_{12} and χ_3-borophene. Firstly, for the diffusion energy barrier, we followed the symmetries of the nanosheets and identified two possible diffusion paths. These paths were carefully chosen based on the most stable neighboring adsorption sites on the nanosheets. We determined that the possible diffusion path would be from one stable adsorption site to the adjacent corresponding sites. As a result, the most common diffusion path for both borophenes is the one following the chain of hollow hexagons. Another path was also considered, which involved crossing the triangle of boron atoms towards the corresponding stable sites. These two paths were strictly considered due to the symmetry of the borophenes (path i and path ii) : For NaO_2 on β_{12}-borophene system (Fig. 4a) and NaO_2 on χ_3-borophene system (Fig. 4b). After the calculations, we found that for NaO_2 on β_{12}-borophene, path-i had diffusion barrier energy of 0.89 eV and path-ii with 1.00 eV (Fig. 4a). Path-i having a lower energy barrier than path-ii suggests that the species easily follows

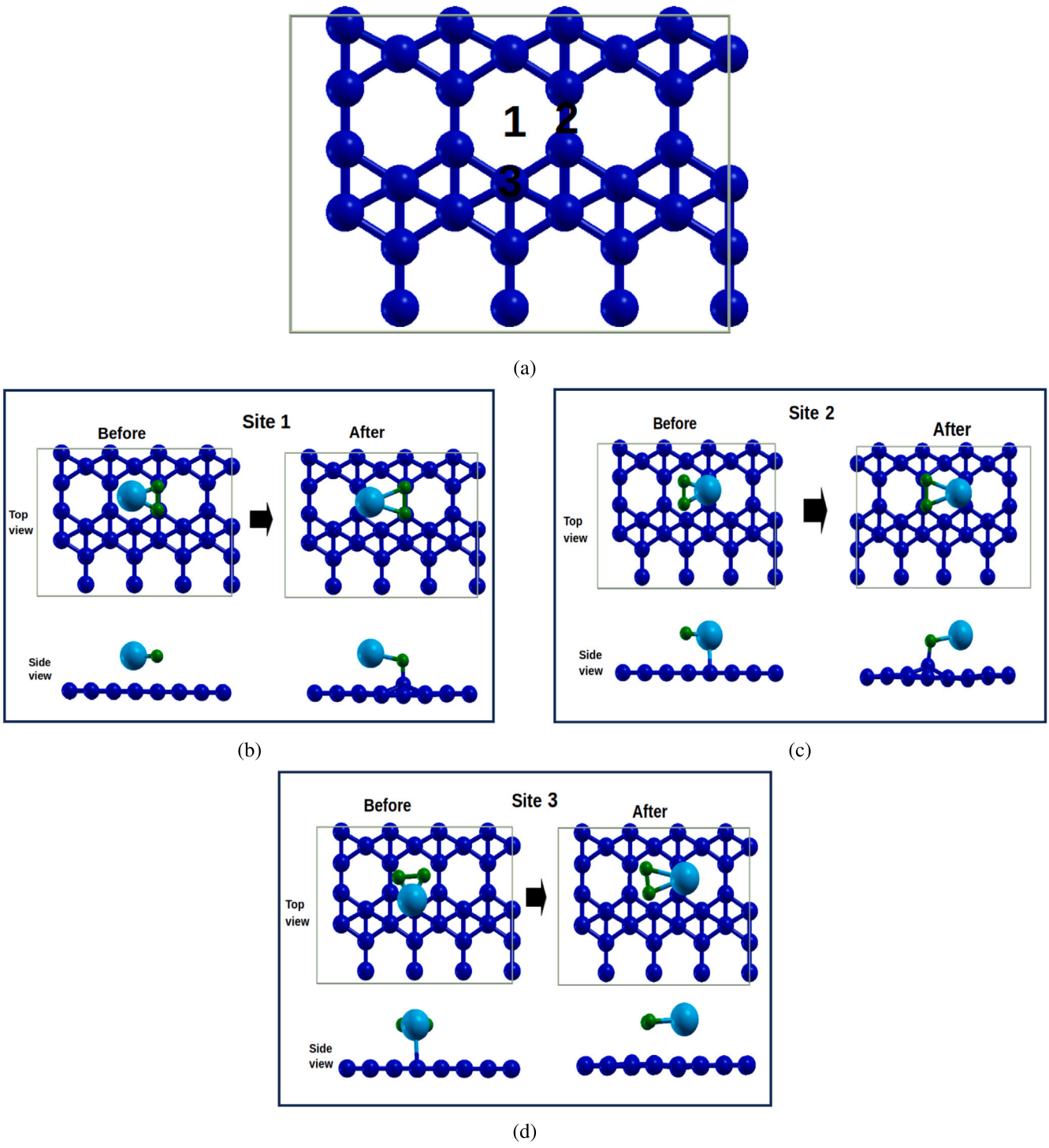

Fig. 3. Before (left) and after (right) simulation of NaO_2 on χ_3-borophene systems: (a) possible adsorption sites on χ_3 borophene (b) top and end views of configuration at Site 1, (c) top and end views of configuration at Site 2, and (d) top and end views of configuration at Site 3. The sodium, oxygen, and boron atoms are denoted by teal, green, and blue colors. (For interpretation of the references to color in this figure legend, the reader is referred to the web version of this article.)

the chain of hollow hexagons. Therefore, the energy barrier of the sodium superoxide on β_{12}-borophene is predicted to be 0.89 eV. Next, for NaO_2 on χ_3-borophene, path-i had an energy barrier of 1.37 eV lower than path-ii with a value of 1.49 eV (Fig. 4b). Also here, we observed that path-i; following the chain of hollow hexagons has a relatively moderate diffusion energy barrier than passing across the triangles of boron atoms (path-ii). According to our comparison of the two systems, it was found that the diffusion energy barrier for NaO_2 on β_{12} borophene is lower compared to NaO_2 on χ_3 borophene (as shown in Table 1). This suggests that the higher adsorption energy of NaO_2 onto the nanosheet results in the higher diffusion energy barrier since the NaO_2 is more strongly anchored onto the β_{12} borophene than it is on the χ_3 borophene. The diffusion energy barriers for the sodium superoxide on borophenes are moderate (Table 2) and are lower than those of other 2D nanosheets such as defective black phosphorus adsorbed with sodium only [52].

In addition to the diffusion energy barriers analysis, we also calculated the energy required to decompose NaO_2 on both nanosheets

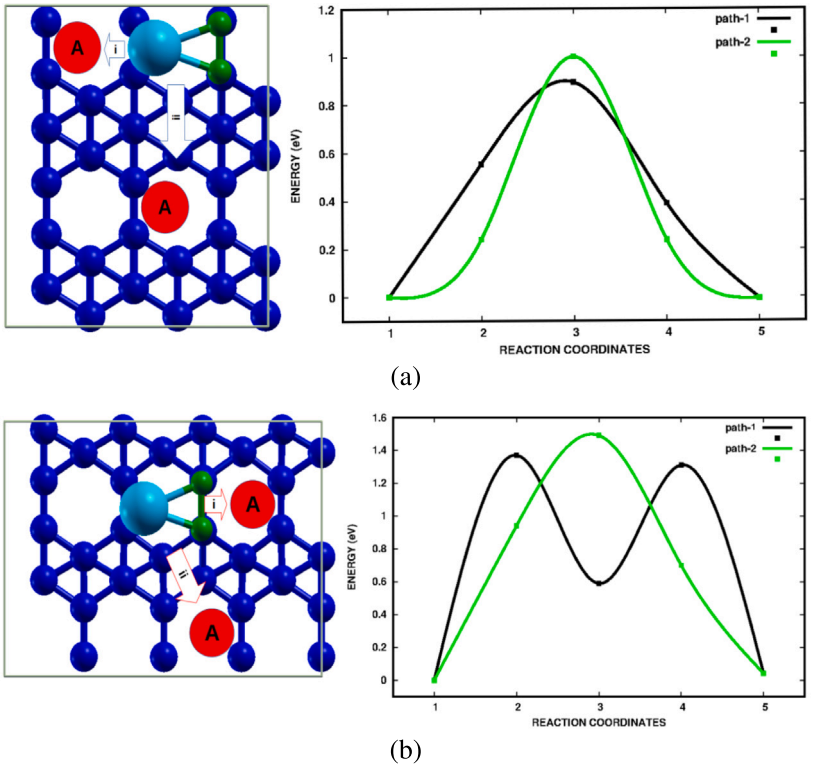

Fig. 4. Plan view of possible diffusion paths and energy profiles of adsorbates on borophenes: (a) NaO_2 on β_{12}-borophene (b) NaO_2 on χ_3 borophene. The adjacent adsorption sites are donated by A in a red circle. (For interpretation of the references to color in this figure legend, the reader is referred to the web version of this article.)

Table 1
The calculated properties of optimized NaO_2 configurations at different sites of β_{12} and χ_3-borophenes: Adsorption energies and binding distances.

System	Adsorption site	Adsorption energy (eV)	Binding-distance (Å)	
			O_2	Na
NaO_2 on β_{12}-borophene	Site 1	−3.85	1.53	2.54
	Site 2	−1.95	2.51	2.55
	Site 3	−1.45	2.46	2.56
	Site 4	−3.80	1.54	2.56
NaO_2 on χ_3-borophene	Site 1	−3.29	1.50	2,53
	Site 2	−3.28	1.51	2.50
	Site 3	−2.04	1.92	2.65

Table 2
Calculated diffusion energy barrier for β_{12} and χ_3-borophenes against sodium superoxide.

System	Diffusion energy barrier (eV)	
	path-i	path-ii
NaO_2 on β_{12}-borophene	0.89	1.00
NaO_2 on χ_3-borophene	1.37	1.49

Table 3
Predicted NaO_2 on β_{12} and χ_3-borophene quantified electric charge density.

System	Electric charge (e)		
	O_2	Na	Borophene
NaO_2 on β_{12}	+1.76	−0.89	−0.87
NaO_2 on χ_3	+1.83	−0.89	−0.94

using the nudged elastic band scheme [50,51]. It is important to note that during the charging process, the adsorbed sodium superoxide undergoes random decomposition. Therefore, to accurately analyze the decomposition energy, the shortest path (Path i) (Fig. 4) with the lowest energy barrier was considered as the only dissociative path. Moreover, to ensure precision, the most stable adsorption sites for NaO_2 were taken into account before dissociation, as well as the stable adsorption sites for O_2 and Na after dissociation (Figs. 5a and 5c). The stable site for NaO_2 was considered the first image, while the sites for isolated O_2 and Na were considered the last image. After conducting calculations, the predicted decomposition energies for NaO_2 on these materials were found to be 0.73 eV (Fig. 5b) and 0.52 eV (Fig. 5d), respectively. This is significant because when compared to the NaO_2 formation energy in a vacuum (3.91 eV), it suggests that these materials have the potential to catalyze the decomposition process. Furthermore, the β_{12} borophene was found to have a higher dissociation energy than the χ_3 borophene, indicating that it can dissociate the NaO_2 faster. Overall, these catalytic effects demonstrate the ability of these nanosheets to improve the flow of species in sodium–oxygen batteries,

3.3.1. Charge density difference distribution

After the calculation of the adsorption energies for the most stable configurations, we obtained a deeper understanding of the electronic interactions in the systems, by determining the distribution of charge density differences and plotting the corresponding charge isosurfaces [53], as shown in Fig. 6. This was achieved using the following equation:

$$\rho_{charge} = \rho_{complex} - \rho_{slab} - \rho_{adsorbate}. \quad (2)$$

Where ρ_{charge} is the charge density difference between the anchored adsorbate and the substrate, $\rho_{complex}$ the charge density of the optimized system (substrate with the adsorbate), ρ_{slab} charge density of the substrate without the adsorbate, and $\rho_{adsorbate}$ charge density of the isolated adsorbate. Here, it should be noted that the atomic positions of the substrate and adsorbate are maintained like in the complex system. Additionally, to get more insight into the quantity of charge transferred, we adopted Bader charge analysis scheme [54,55] and quantitatively calculated the charge density (Table 3).

Firstly, for the system of NaO_2 on β_{12}-borophene (Fig. 6a), charge accumulated (purple) towards the β_{12}-borophene sodium and transferring

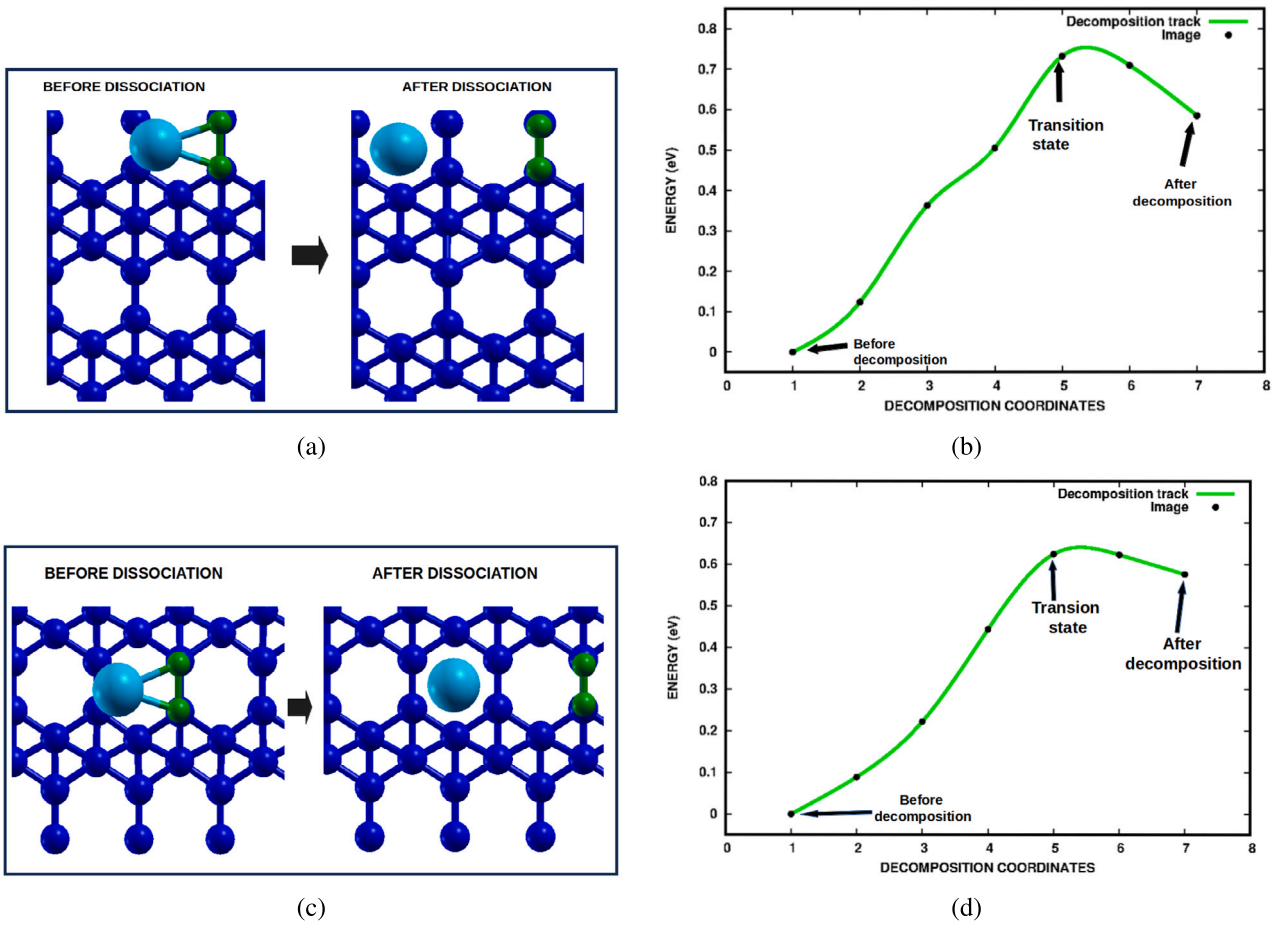

Fig. 5. Top views of possible decomposition paths and energy profiles: (a–b) NaO_2 on β_{12}-borophene, and (c–d) NaO_2 on χ_3 borophene. The black dots denote decomposition images and the green curve represents the decomposition energy path. (For interpretation of the references to color in this figure legend, the reader is referred to the web version of this article.)

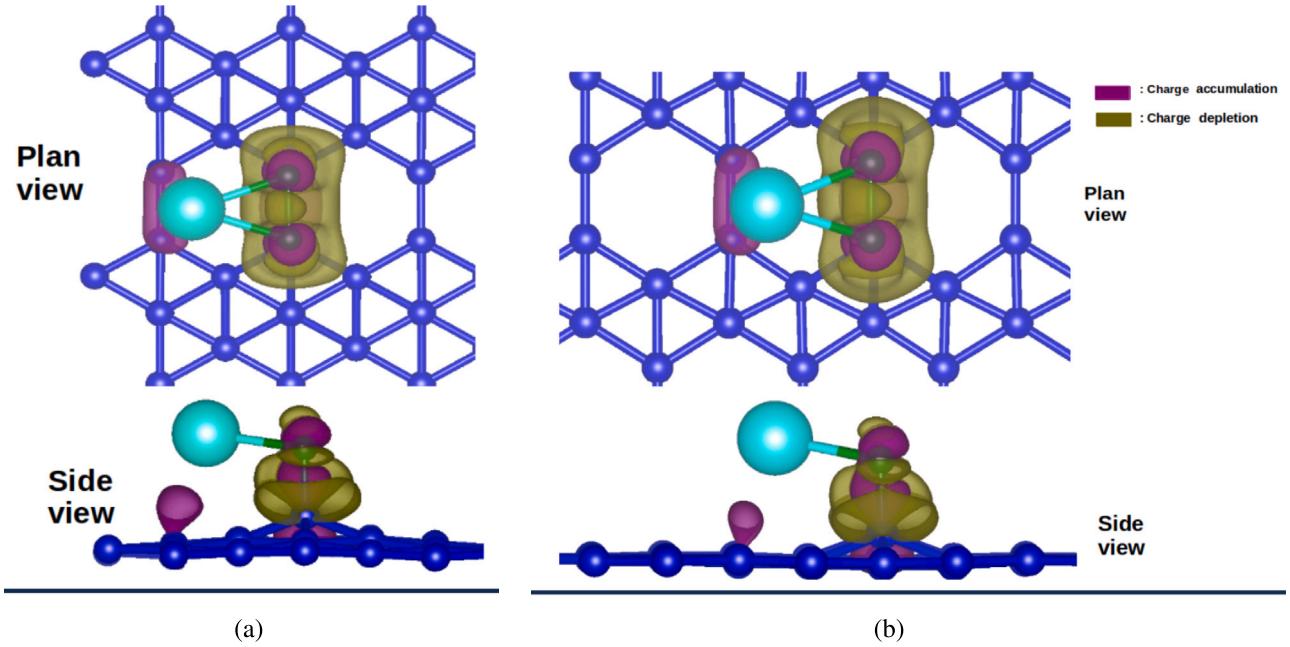

Fig. 6. Charge density distribution between sodium superoxide (NaO_2) **and borophenes:** (a) Charge transfer between NaO_2 and β_{12}-borophene (b) Charge transfer between NaO_2 and χ_3-borophene: Where isosurfaces are denoted by color purple and brown for charge accumulation and depletion, respectively. (For interpretation of the references to color in this figure legend, the reader is referred to the web version of this article.)

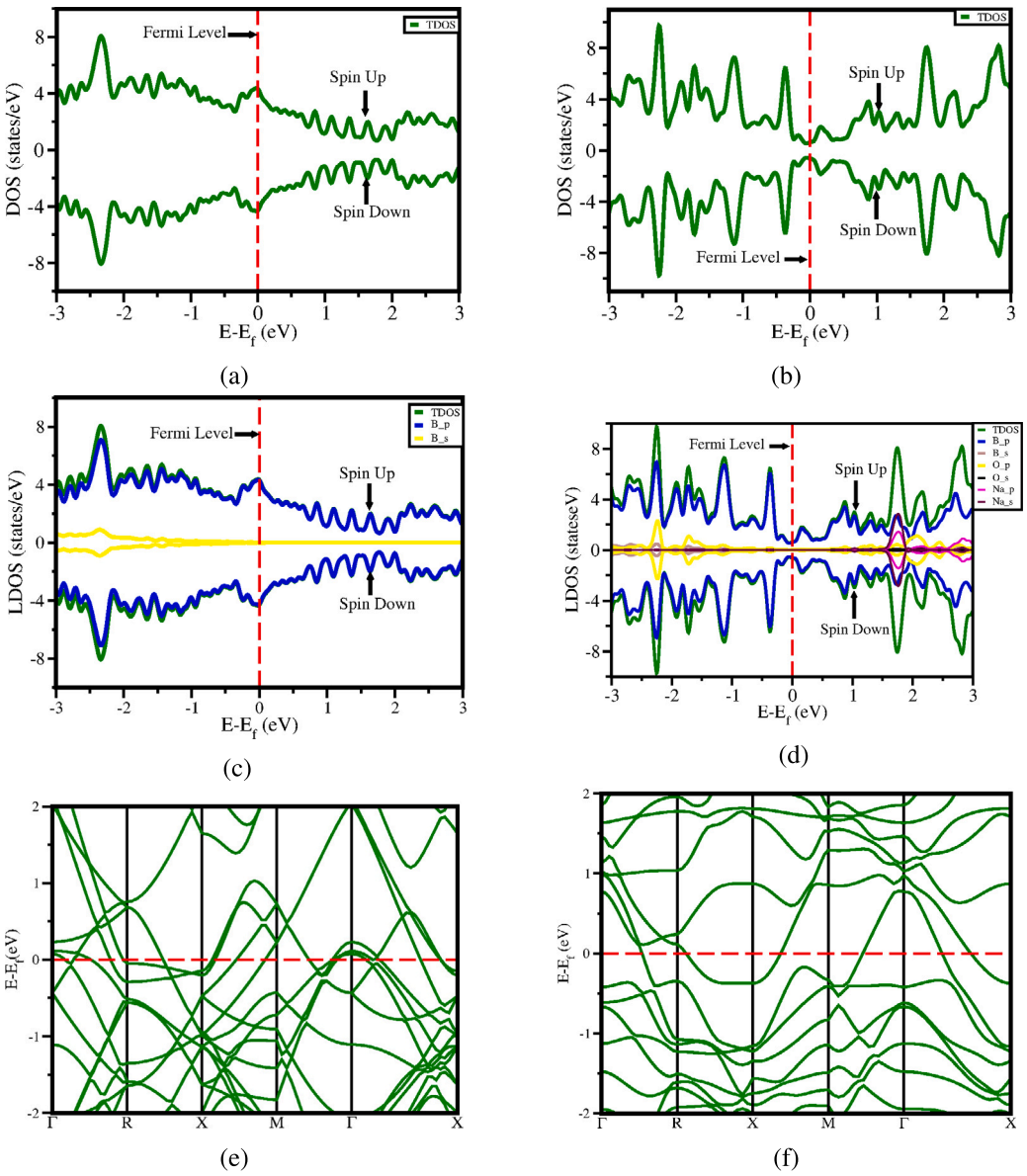

Fig. 7. Spin polarized density of states and bands structures: (a–b) total density of states (TDOS) for pristine and NaO_2 on β_{12}-borophene system, (c–d) local density of states (LDOS) for pristine and NaO_2 on β_{12}-borophene: (e–f) bands structures for pristine and NaO_2 on β_{12}-borophene. A dashed red line denotes the Fermi level.

about 0.89 |e| of charge. On the other side, charge depleted (brown) from the β_{12}-borophene and accumulated (purple) towards the oxygen atoms. Hence, the quantity of charge shared was 1.76 |e|. This big value of charge shared furthermore confirmed the formed covalent bonds. Therefore, the overall charge transfer between the β_{12}-borophene and sodium superoxide was 0.87 |e|.

Next, for the NaO_2 on χ_3-borophene (Fig. 6b), a similar trend was observed as in the previous system. The charge accumulated (purple) towards the χ_3-borophene, with the charge of 0.89 |e| being transferred. Additionally, charge depleted (brown) from the χ_3-borophene and accumulated (purple) towards the oxygen atoms, and a quantity of 1.83 |e| was shared. Hence, a total quantified charge of 0.94 |e| was transferred between the NaO_2 and χ_3-borophene. Most interestingly, the charge transferred between NaO_2 and χ_3-borophene was larger as compared to the one transferred between the NaO_2 and the β_{12}-borophene (Table 3). This observation was intriguing as the adsorption energy for the NaO_2 on β_{12}-borophene was determined to be higher than NaO_2 on χ_3-borophene (Table 1).

3.4. Conductivity characteristics of β_{12} and χ_3-borophenes with adsorbed NaO_2

To utilize a material as an electrode, it is important to consider its conductivity characteristics. Therefore, these properties were determined by calculating the total density of states (TDOS), the local density of states (LDOS), and band structures before and after adsorbing sodium superoxides. Our results indicated that both pristine free-standing borophenes exhibit metallic characteristics, confirmed by the overlapping bands of the valency and conduction, which suggest a zero band gap and excellent electronic conductivity. We observed this trend for the pristine of β_{12}-borophene (Figs. 7a, 7c and 7e) and χ_3-borophene (Figs. 8a, 8c and 8e). The 2p-orbitals boron atom dominated the orbital contributions along the Fermi level for both crystals, with minimal contributions from 2s-orbitals. The high orbitals states along the Fermi level demonstrate the presence of more occupied electronic states, implying the easy flow of electrons between the valency and conduction bands. Our results are consistent with previously reported works [49,56]. These results are the benchmark. Hence, we introduced

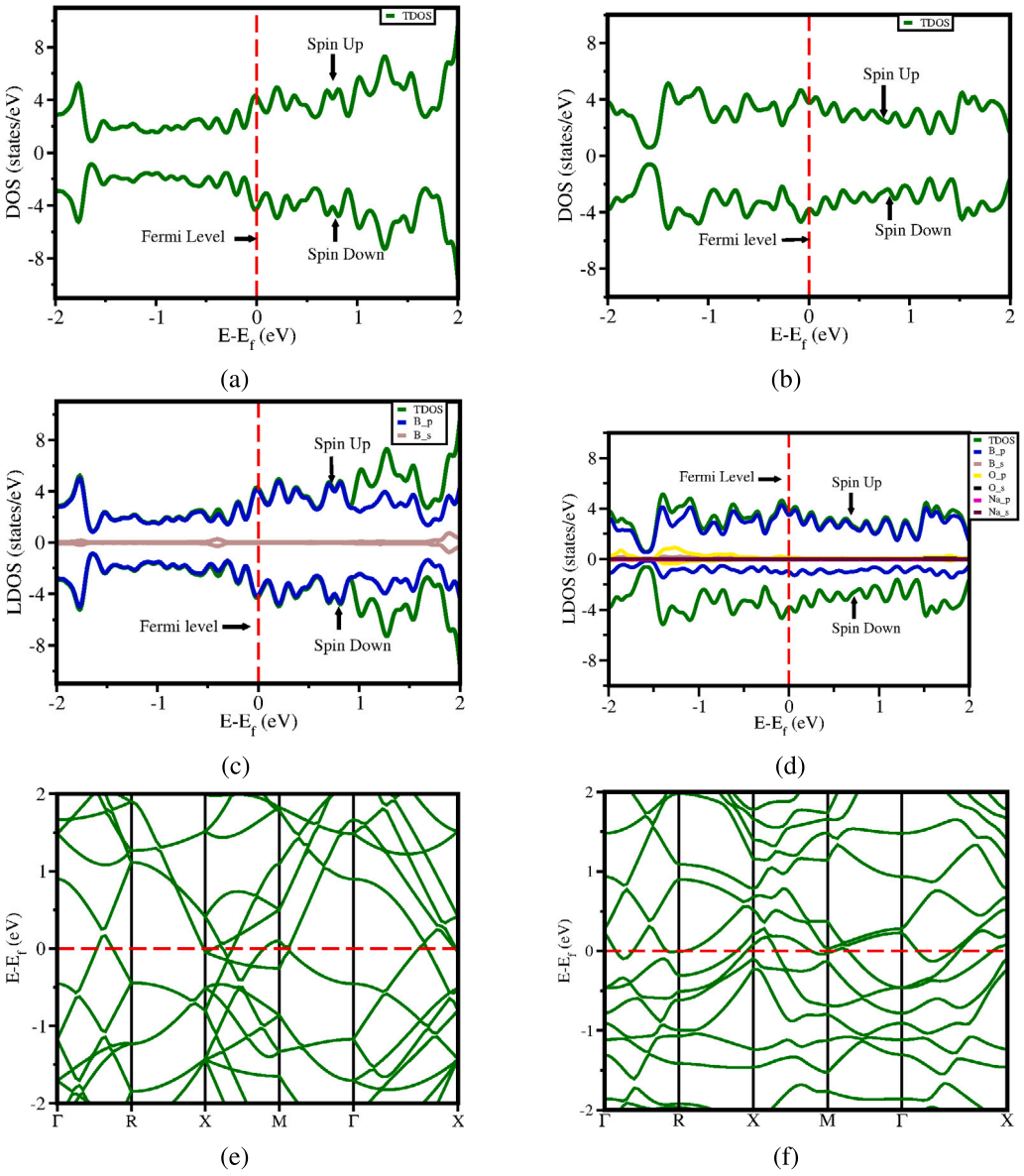

Fig. 8. Spin polarized density of states and bands structures: (a–b) total density of states (TDOS) for pristine and NaO_2 on χ_3-borophene system, (c–d) local density of states (LDOS) for pristine and NaO_2 on χ_3-borophene, (e–f) bands structures of pristine and NaO_2 on χ_3-borophene. A dashed red line denotes the Fermi level.

the adsorbate on the crystal structures. Firstly, when sodium superoxide was introduced onto the β_{12}-borophene, we observed bands moving upwards as the Fermi level shifted downwards (Fig. 7f). This is due to the high electronegativity of oxygen in the NaO_2, which left many unoccupied electronic states in the substrate (Figs. 7b and 7d). Despite the decrease in the orbital states around the Fermi level, the system did not have a zero band gap. As shown in Fig. 7d, total orbital contributions were dominated by the 2p-orbitals of the boron atoms and minimal contributions from 3s- and 2p-orbitals of Na and O_2, respectively. The electronic structure of the material retained its metallic characteristics, as compared to the pristine.

In contrast to the previous system, we observed an increase in the orbitals states along the Fermi level for NaO_2 on χ_3-borophene (Figs. 8b and 8d). This increase in orbital concentration indicates enhanced electronic conductivity, enabling electrons to diffuse freely between the valence and conduction bands. For the local orbital contributions, the majority came from the 2p-orbitals of the boron atoms and minimal from the 2p-orbitals of the oxygen (Fig. 8d). Additionally, as the Fermi level shifted upwards, bands had moved downward (Fig. 8f) due to the charge (electrons) from the NaO_2. Although hybridization occurred, it did not alter or destroy the metallic characteristics of the material.

Upon analyzing the adsorption of NaO_2 on the borophenes, the electronic states along the Fermi level shrank significantly in the NaO_2 on β_{12} borophene system. This could be due to the strong hybridization between the β_{12} borophene and the NaO_2 orbitals, which resulted in a highly altered orbital concentration along the Fermi level and supports the obtained strong adsorption energy of NaO_2 on the β_{12} borophene (Table 1). On the other hand, in the NaO_2 on χ_3 borophene system, the electronic states along the Fermi level were not strongly altered compared to the previous system. This is because the hybridization was not as strong as for NaO_2 on β_{12} borophene. Ultimately, there was preservation of the electrical conductivity in both borophenes.

4. Conclusions

In conclusion, using density functional theory we investigated the adsorption mechanisms of sodium superoxide (NaO_2) on the β_{12} and χ_3-borophenes. Our results showed that; the adsorption energies for sodium superoxide on β_{12} and χ_3 borophenes are −3.85 eV and −3.29

eV, respectively, suggesting a strong anchoring power from both structures. This is important as it suggests that the materials have a high retention of the NaO_2 during the discharging process, thereby preventing them from desorbing or decomposing into the electrolyte. Furthermore, the β_{12} and χ_3 structures showed moderate diffusion energy barriers of 0.89 eV and 1.37 eV and decomposition energies of 0.73 eV and 0.52 eV, respectively. Moreover, the relatively moderate diffusion energy barriers and the lower decomposition energies than NaO_2 formation energy (3.90 eV) in a vacuum. suggest nanosheets catalytic effects on the migration and decomposition of the NaO_2 into sodium (Na^+) and oxygen (O_2). It is worth noting that both structures maintained their metallic characteristics after adsorbing NaO_2. This is significant because, during the charging process species should be charged back and prevent dendrite formation at the cathode electrode surface, thereby enhancing the cycling life of the battery. Ultimately, the predicted electronic properties of β_{12} and χ_3-borophene demonstrate their potential as cathode electrode materials for the performance of sodium–oxygen batteries. As our work was solely conducted at ground state (0 K), in future research works, we recommend examining the effects of temperature variation on the predicted electronic properties. This is significant as batteries operate at different temperatures and environments.

CRediT authorship contribution statement

C. Fwalo: Writing – original draft, Visualization, Validation, Software, Methodology, Investigation, Formal analysis, Conceptualization. **A. Kochaev:** Validation, Methodology, Conceptualization. **R.E. Mapasha:** Validation, Supervision, Resources, Funding acquisition.

Declaration of competing interest

The authors declared no any conflicting interest that may influence the outcome of the results.

Data availability

Data will be made available on request.

Acknowledgments

This research project was made possible through the financial support from the University of Pretoria, Department of Research and Innovation. Furthermore, we are grateful for the computational resource support (Project name: MATS1429) from the Center of High-Performance Computing (CHPC) in Cape Town, South Africa. R.E.M. thanks the National Institute for Theoretical and Computational Sciences (NTheCS) for the financial support.

References

[1] T. Placke, R. Kloepsch, S. Dühnen, M. Winter, Lithium ion, lithium metal, and alternative rechargeable battery technologies: the odyssey for high energy density, J. Solid State Electrochem. 21 (2017) 1939–1964.
[2] Y. Liang, C.-Z. Zhao, H. Yuan, Y. Chen, W. Zhang, J.-Q. Huang, D. Yu, Y. Liu, M.-M. Titirici, Y.-L. Chueh, et al., A review of rechargeable batteries for portable electronic devices, InfoMat 1 (1) (2019) 6–32.
[3] G. Berckmans, M. Messagie, J. Smekens, N. Omar, L. Vanhaverbeke, J. Van Mierlo, Cost projection of state of the art lithium-ion batteries for electric vehicles up to 2030, Energies 10 (9) (2017) 1314.
[4] J.W. Choi, D. Aurbach, Promise and reality of post-lithium-ion batteries with high energy densities, Nature Rev. Mater. 1 (4) (2016) 1–16.
[5] T. Liu, J.P. Vivek, E.W. Zhao, J. Lei, N. Garcia-Araez, C.P. Grey, Current challenges and routes forward for nonaqueous lithium–air batteries, Chem. Rev. 120 (14) (2020) 6558–6625.
[6] C. Xia, C. Kwok, L. Nazar, A high-energy-density lithium-oxygen battery based on a reversible four-electron conversion to lithium oxide, Science 361 (6404) (2018) 777–781.
[7] D. Aurbach, B.D. McCloskey, L.F. Nazar, P.G. Bruce, Advances in understanding mechanisms underpinning lithium–air batteries, Nature Energy 1 (9) (2016) 1–11.
[8] P. Tan, H. Jiang, X. Zhu, L. An, C. Jung, M. Wu, L. Shi, W. Shyy, T. Zhao, Advances and challenges in lithium-air batteries, Appl. Energy 204 (2017) 780–806.
[9] P. Hartmann, C.L. Bender, M. Vračar, A.K. Dürr, A. Garsuch, J. Janek, P. Adelhelm, A rechargeable room-temperature sodium superoxide (NaO2) battery, Nature Mater. 12 (3) (2013) 228–232.
[10] H. Yadegari, X. Sun, Sodium–oxygen batteries: recent developments and remaining challenges, Trends Chem. 2 (3) (2020) 241–253.
[11] F.W. Clarke, H.S. Washington, The Composition of the Earth's Crust, Vol. 127, US Government Printing Office, 1924.
[12] O. Arcelus, C. Li, T. Rojo, J. Carrasco, Electronic structure of sodium superoxide bulk,(100) surface, and clusters using hybrid density functional: Relevance for Na–O2 batteries, J. Phys. Chem. Lett. 6 (11) (2015) 2027–2031.
[13] N. Chawla, M. Safa, Sodium batteries: A review on sodium-sulfur and sodium-air batteries, Electronics 8 (10) (2019) 1201.
[14] J.H. Kim, J.H. Jeong, N. Kim, R. Joshi, G.-H. Lee, Mechanical properties of two-dimensional materials and their applications, J. Phys. D: Appl. Phys. 52 (8) (2018) 083001.
[15] D. Akinwande, C.J. Brennan, J.S. Bunch, P. Egberts, J.R. Felts, H. Gao, R. Huang, J.-S. Kim, T. Li, Y. Li, et al., A review on mechanics and mechanical properties of 2D materials—Graphene and beyond, Extreme Mech. Lett. 13 (2017) 42–77.
[16] P. Avouris, C. Dimitrakopoulos, Graphene: synthesis and applications, Mater. Today 15 (3) (2012) 86–97.
[17] X. Cai, L. Lai, Z. Shen, J. Lin, Graphene and graphene-based composites as Li-ion battery electrode materials and their application in full cells, J. Mater. Chem. A 5 (30) (2017) 15423–15446.
[18] S. Angizi, S.A.A. Alem, A. Pakdel, Towards integration of two-dimensional hexagonal boron nitride (2D h-BN) in energy conversion and storage devices, Energies 15 (3) (2022) 1162.
[19] K. Zhang, Y. Feng, F. Wang, Z. Yang, J. Wang, Two dimensional hexagonal boron nitride (2D-hBN): synthesis, properties and applications, J. Mater. Chem. C 5 (46) (2017) 11992–12022.
[20] M. Naguib, M.W. Barsoum, Y. Gogotsi, Ten years of progress in the synthesis and development of MXenes, Adv. Mater. 33 (39) (2021) 2103393.
[21] F. Ming, H. Liang, G. Huang, Z. Bayhan, H.N. Alshareef, Mxenes for rechargeable batteries beyond the lithium-ion, Adv. Mater. 33 (1) (2021) 2004039.
[22] A.J. Mannix, X.-F. Zhou, B. Kiraly, J.D. Wood, D. Alducin, B.D. Myers, X. Liu, B.L. Fisher, U. Santiago, J.R. Guest, et al., Synthesis of borophenes: Anisotropic, two-dimensional boron polymorphs, Science 350 (6267) (2015) 1513–1516.
[23] A. Rubab, N. Baig, M. Sher, M. Sohail, Advances in ultrathin borophene materials, Chem. Eng. J. 401 (2020) 126109.
[24] B. Feng, J. Zhang, Q. Zhong, W. Li, S. Li, H. Li, P. Cheng, S. Meng, L. Chen, K. Wu, Experimental realization of two-dimensional boron sheets, Nature Chem. 8 (6) (2016) 563–568.
[25] B. Peng, H. Zhang, H. Shao, Z. Ning, Y. Xu, G. Ni, H. Lu, D.W. Zhang, H. Zhu, Stability and strength of atomically thin borophene from first principles calculations, Mater. Res. Lett. 5 (6) (2017) 399–407.
[26] Z. Xie, X. Meng, X. Li, W. Liang, W. Huang, K. Chen, J. Chen, C. Xing, M. Qiu, B. Zhang, et al., Two-dimensional borophene: properties, fabrication, and promising applications, Research (2020).
[27] M. Ou, X. Wang, L. Yu, C. Liu, W. Tao, X. Ji, L. Mei, The emergence and evolution of borophene, Adv. Sci. 8 (12) (2021) 2001801.
[28] B. Mortazavi, O. Rahaman, S. Ahzi, T. Rabczuk, Flat borophene films as anode materials for Mg, Na or Li-ion batteries with ultra high capacities: a first-principles study, Appl. Mater. Today 8 (2017) 60–67.
[29] J. Liu, L. Zhang, L. Xu, Theoretical prediction of borophene monolayer as anode materials for high-performance lithium-ion batteries, Ionics 24 (2018) 1603–1615.
[30] L.T. Ta, I. Hamada, Y. Morikawa, V.A. Dinh, Adsorption of toxic gases on borophene: surface deformation links to chemisorptions, RSC Adv. 11 (30) (2021) 18279–18287.
[31] J.-X. Duan, Y.-P. Tian, C.-B. Wang, L.-L. Zhang, First-principles study of χ3-borophene as a candidate for gas sensing and the removal of harmful gases, Nanomaterials 13 (14) (2023) 2117.
[32] F. Zergani, Z. Tavangar, Gas sensing behavior and adsorption mechanism on χ3 borophene surface, Chem. Eng. J. 431 (2022) 133947.
[33] X. Xu, R. Si, Y. Dong, L. Li, M. Zhang, X. Wu, J. Zhang, K. Fu, Y. Guo, Y. He, Borophene- supported single transition metal atoms as potential oxygen evolution/reduction electrocatalysts: a density functional theory study, J. Mol. Model. 27 (2021) 1–10.
[34] L. Zhang, P. Liang, H.-b. Shu, X.-l. Man, F. Li, J. Huang, Q.-m. Dong, D.-l. Chao, Borophene as efficient sulfur hosts for lithium–sulfur batteries: suppressing shuttle effect and improving conductivity, J. Phys. Chem. C 121 (29) (2017) 15549–15555.
[35] H. Jiang, W. Shyy, M. Liu, Y. Ren, T. Zhao, Borophene and defective borophene as potential anchoring materials for lithium–sulfur batteries: a first-principles study, J. Mater. Chem. A 6 (5) (2018) 2107–2114.

[36] S. Grixti, S. Mukherjee, C.V. Singh, Two-dimensional boron as an impressive lithium-sulphur battery cathode material, Energy Storage Mater. 13 (2018) 80–87.
[37] X. Zhang, J. Hu, Y. Cheng, H.Y. Yang, Y. Yao, S.A. Yang, Borophene as an extremely high capacity electrode material for Li-ion and Na-ion batteries, Nanoscale 8 (33) (2016) 15340–15347.
[38] P. Giannozzi, O. Andreussi, T. Brumme, O. Bunau, M.B. Nardelli, M. Calandra, R. Car, C. Cavazzoni, D. Ceresoli, M. Cococcioni, et al., Advanced capabilities for materials modelling with Quantum ESPRESSO, J. Phys.: Condens. Matter 29 (46) (2017) 465901.
[39] S. Grimme, Semiempirical GGA-type density functional constructed with a long-range dispersion correction, J. Comput. Chem. 27 (15) (2006) 1787–1799.
[40] J.P. Perdew, K. Burke, M. Ernzerhof, Perdew, burke, and ernzerhof reply, Phys. Rev. Lett. 80 (4) (1998) 891.
[41] P.E. Blöchl, Projector augmented-wave method, Phys. Rev. B 50 (24) (1994) 17953.
[42] H.J. Monkhorst, J.D. Pack, Special points for Brillouin-zone integrations, Phys. Rev. B 13 (12) (1976) 5188.
[43] D.J. Chadi, Special points for Brillouin-zone integrations, Phys. Rev. B 16 (4) (1977) 1746.
[44] M. Methfessel, A. Paxton, High-precision sampling for Brillouin-zone integration in metals, Phys. Rev. B 40 (6) (1989) 3616.
[45] S. Ehrlich, J. Moellmann, W. Reckien, T. Bredow, S. Grimme, System-dependent dispersion coefficients for the DFT-D3 treatment of adsorption processes on ionic surfaces, ChemPhysChem 12 (17) (2011) 3414–3420.
[46] S. Karimzadeh, B. Safaei, T.-C. Jen, Investigation on electrochemical performance of striped, β12 and χ3 Borophene as anode materials for lithium-ion batteries, J. Mol. Graph. Model. 120 (2023) 108423.
[47] S. Grixti, S. Mukherjee, C.V. Singh, Two-dimensional boron as an impressive lithium-sulphur battery cathode material, Energy Storage Mater. 13 (2018) 80–87.
[48] B. Feng, J. Zhang, Q. Zhong, W. Li, S. Li, H. Li, P. Cheng, S. Meng, L. Chen, K. Wu, Experimental realization of two-dimensional boron sheets, Nature Chem. 8 (6) (2016) 563–568.
[49] D. Li, J. Gao, P. Cheng, J. He, Y. Yin, Y. Hu, L. Chen, Y. Cheng, J. Zhao, 2D boron sheets: structure, growth, and electronic and thermal transport properties, Adv. Funct. Mater. 30 (8) (2020) 1904349.
[50] G. Henkelman, H. Jónsson, Improved tangent estimate in the nudged elastic band method for finding minimum energy paths and saddle points, J. Chem. Phys. 113 (22) (2000) 9978–9985.
[51] H. Jónsson, G. Mills, K.W. Jacobsen, Nudged elastic band method for finding minimum energy paths of transitions, in: Classical and Quantum Dynamics in Condensed Phase Simulations, World Scientific, 1998, pp. 385–404.
[52] X. Sun, Z. Wang, Sodium adsorption and diffusion on monolayer black phosphorus with intrinsic defects, Appl. Surf. Sci. 427 (2018) 189–197.
[53] Y. Wang, W.Y. Wang, L.-Q. Chen, Z.-K. Liu, Bonding charge density from atomic perturbations, J. Comput. Chem. 36 (13) (2015) 1008–1014.
[54] W. Tang, E. Sanville, G. Henkelman, A grid-based Bader analysis algorithm without lattice bias, J. Phys.: Condens. Matter 21 (8) (2009) 084204.
[55] G. Henkelman, A. Arnaldsson, H. Jónsson, A fast and robust algorithm for Bader decomposition of charge density, Comput. Mater. Sci. 36 (3) (2006) 354–360.
[56] X. Sun, X. Liu, J. Yin, J. Yu, Y. Li, Y. Hang, X. Zhou, M. Yu, J. Li, G. Tai, et al., Two-dimensional boron crystals: structural stability, tunable properties, fabrications and applications, Adv. Funct. Mater. 27 (19) (2017) 1603300.